Ray tracing of penetrating chorus and its implications for the radiation belts

J. Bortnik, R. M. Thorne

Department of Atmospheric and Oceanic Sciences, University of California,

Los Angeles, California, USA.

N. P. Meredith

British Antarctic Survey, Natural Environment Research Council,

Cambridge, UK.

O. Santolik

Faculty of Mathematics and Physics, Charles University, Prague and

IAP/ASCR, Prague, Czech Republic.

J. Bortnik, and R. M. Thorne, Department of Atmospheric and Oceanic Sciences, University of California, Los Angeles, CA 90095-1565, USA. (jbortnik@gmail.com, rmt@atmos.ucla.edu)

N. P. Meredith, British Antarctic Survey, Natural Environment Research Council, Madingley Road, Cambridge, CB3 0ET, UK. (nmer@bas.ac.uk)

O. Santolik, Faculty of Mathematics and Physics, Charles University, Prague and IAP/ASCR, Prague, Czech Republic. (ondrej.santolik@mff.cuni.cz)

Using ray tracing and suprathermal electron distributions from CRRES, the final propagation latitudes of typical chorus rays are calculated as a function of L, MLT, AE, and initial wave normal angle. Rays initiated within a certain range of wave normals $\psi_P \sim -0.8\psi_G$ to $-0.6\psi_G$ (where ψ_G is the Gendrin angle) propagate to very high latitudes, largely avoiding Landau damping whilst remaining roughly field-aligned for large portions of their propagation paths. The relative wave power of such penetrating chorus may increase above its initial value due to the low damping rates and magnetic field line convergence. By considering 4 representative rays with $f = 0.3 f_{ce}$, and calculating the resonant energies at the edge of the loss-cone, it is shown that penetrating chorus readily interacts with electrons in the > 1 MeV energy range, and may thus contribute to the previously reported relativistic electron microbursts.

1. Introduction

Chorus waves are intense, naturally-generated electromagnetic emissions, typically occurring outside the plasmapause, in the magnetic local time (MLT) range $\sim 23-15$h, with frequencies of $\sim 0.1-10$ kHz [*Meredith et al.*, 2001; *Santolik et al.*, 2004]. Interest in chorus has recently increased due to the recognition of this wave's importance in controlling radiation-belt dynamics [e.g., *Horne and Thorne*, 2003; *Horne et al.*, 2005; *Thorne et al.* 2005; *Meredith et al.*, 2002]. Chorus can act as a mediating agent, transferring energy from the lower energy ($\sim 10-100$ keV) electrons which are predominantly precipitated, to the relativistic (~ 1 MeV) electrons which are predominantly accelerated [e.g. *Meredith et al.*, 2002; *Horne and Thorne*, 2003; *Horne et al.*, 2005]. Since the pitch-angle and energy diffusion rates used in studying radiation-belt dynamics are critically dependent on the chorus wave power distribution and wave normal characteristics, accurate knowledge of the propagation of chorus waves (power, damping, wave normal evolution, etc.) is essential for an accurate evaluation.

In the present paper, the effects of suprathermal electron fluxes (which lead to Landau damping) upon chorus propagation are examined using a combination of measured fluxes, and ray tracing. Section 2 summarizes our methodology, and Section 3 presents the results of ray tracing, investigating the dependence of chorus propagation on the initial wave normal angle. In Section 4 the ray tracing results are related to energetic electron scattering, and Section 5 summarizes our findings.

2. Methodology

The methodology used to investigate the propagation characteristics and damping of chorus waves has been described in detail by *Bortnik et al.* [2007], and consists of 3 steps:

1. *Suprathermal electron distribution*: Suprathermal electron flux observations from CRRES were used to create statistical distributions as a function of L-shell ($L = 1$ to 7, in $0.1L$ bins), MLT (in 1 hour bins), and AE (in 3 bins: quiet AE $<$ 100 nT, moderate 100 $<$ AE $<$ 300 nT, and disturbed AE $>$ 300 nT), in 4 energy channels: 0.213, 1.09, 4.25, and 16.5 keV. Only flux measurements outside the plasmapause were included consistent with typical chorus wave location (see *Meredith et al.* [2004] for the sorting criterion).

2. *Parameter fitting*: For each L, MLT, and AE bin, the 4 flux values (i.e., the 4 energy channels above) were fitted with an assumed (isotropic) phase space density function of the form $f(v) = A_N/v^n$.

3. *Ray tracing and Landau damping*: The set of functions $f(v)$ were used to calculate the Landau damping rates [*Brinca*, 1972] of rays injected at the geomagnetic equator [*Santolik et al.*, 2004] from the appropriate (L, MLT) bin. The equatorial electron density was modeled with a plasmapause located at $L \sim 2.5$ (reflecting disturbed conditions, $\mathrm{Kp}_{\mathrm{max}} \sim 6.7$) after *Carpenter and Anderson* [1992], with off-equatorial density distributed according to the diffusive equilibrium model [*Angerami and Thomas*, 1964], and a dipole magnetic field. The Stanford VLF ray tracing program [*Inan and Bell*, 1977] was used in the computation of the ray paths. Magnetic field line convergence is included by multiplying the local power density by the ratio of azimuthal arc-lengths at the ray versus the initial value, $r_0 \cos(\lambda_0)/r \cos(\lambda)$, where r and λ are the radial distance and latitude of the ray and the subscript '0' represents initial values.

A typical chorus ray path (see legend) is shown in Figure 1a. The fitted electron distribution $f(v)$ (at the chosen L-MLT location) was used to calculate the path-integrated Landau damping, shown together with the ray latitude as a function of group time in Figure 1b. We define the ray termination point when the ray power reaches 1% of its initial value, which defines the ray lifetime (τ_f), final latitude (λ_f), and final distance (d_f). The evolution of the wave normal angle $\psi(\lambda)$ as a function of latitude is shown in panel (c) indicating that even though the ray is injected with $\psi_0 = 0°$, it quickly becomes oblique leading to severe damping.

In the following section the effect of varying ψ_0 upon λ_f is investigated. The angle ψ_0 is normalized to the Gendrin angle ψ_G (the value of ψ at which the group vector becomes field aligned, calculated using *Bortnik et al.* [2006a], Eq. (1)) and varied from (Earthward directed) $-1\psi_G$ to (antiEarthward directed) $+1\psi_G$ in steps of $0.2\psi_G$. These ψ_0 values, their group rays, and the refractive index surface are shown in Figure 1d.

3. Results

A summary of final latitude λ_f(MLT,L) is shown in Figure 2, parameterized by geomagnetic activity and ψ_0. Each ray is injected at $\lambda = 0°$, $f = 0.3 f_{\text{ce}}$. The common colorbar for λ_f is given at the bottom of the figure.

The principal properties of the chorus distribution are:

- The tendency of λ_f to decrease with increasing L, due to the lower ratio between Landau resonant suprathermal particles and cold particles (n_h/n_0).

- The effect of geomagnetic activity upon the MLT distribution of λ_f. As AE increases, for a given L, λ_f becomes progressively more asymmetric with MLT, with maximum λ_f on the day-side, consistent with observational results.

- The agreement of the observed statistical distribution of chorus wave power with those rays originating at essentially field-aligned ($\psi_0 = 0°$) directions [*Bortnik et al.*, 2007].

Figure 2 shows that the Landau damping of chorus is strongly dependent upon ψ_0. For $\psi_0 \geq 0°$, the degree of Landau damping increases and λ_f becomes progressively smaller with increasing ψ_0. However, when $\psi_0 \leq 0°$, λ_f increases dramatically. At $\psi_0 \sim -0.6\psi_G$, $\lambda_f(L < 6) > 60°$ and the wave penetrates to very low altitudes (henceforth referred to as 'penetrating chorus'). As ψ_0 is decreased further, λ_f decreases, and at $\psi_0 = -1\psi_G$ it is sensitively dependent upon $f(v)$, becoming either very large ($\lambda_f > 60°$) at low L and in some parts of the afternoon sector, or very short ($\lambda_f < 10°$) elsewhere, with few intermediate values.

To examine the development of penetrating chorus, 4 rays are plotted in Figure 3. Columns (A)-(D), correspond to rays injected at $L = 4.45$, $f = 0.3f_{\mathrm{ce}}$, MLT = 9.5 h, AE > 300 nT, with $\psi_0 = -1\psi_G$, $-0.65\psi_G$, $0.0\psi_G$, and $+0.5\psi_G$ respectively. The top row (a), shows ray paths in red and wave normal vectors as short black line-segments attached to the ray path. Rows (b) and (c) show the corresponding damping as a function of group time, and $\psi(\lambda)$ respectively. For $\psi_0 = -\psi_G$ the initial damping is very severe, and $\lambda_f = 2.9°$. For $\psi_0 = -0.65\psi_G$, although the initial Landau damping is relatively strong, it is substantially weaker than case (A), and avoids being extinguished close to its origin. The wave normal becomes field-aligned near $\lambda \sim 18°$ (no Landau damping), and the wave power subsequently increases due to field line convergence. In addition, the ray propagates in such a way that ψ remains low and the wave can reach the ionosphere approximately field-aligned. When ψ_0 is increased further (columns (C),(D)), $\psi(\lambda)$ quickly rotates anti-Earthward as it propagates, resulting in severe damping and decreasing λ_f.

Our results indicate that waves injected over a limited range of ψ_0 are able to avoid both the initial intense Landau damping (c.f. column (A)), and the mid-latitude damping (c.f. columns (C) and (D)). From column (B) and Figure 2, the range of penetrating chorus initial angles is $\psi_P \sim -0.8\psi_G$ to $-0.6\psi_G$. Moreover, the final wave normal angle $\psi(\lambda_f)$ is sensitively dependent upon ψ_0. At some critical angle ψ_B (bifurcation angle [*Thorne and Kennel*, 1967; *Chum and Santolik*, 2005]) within the ψ_P range, $\psi(\lambda_f) \sim 0°$ (also close to local vertical at high latitudes) and the ray is able (in principle) to propagate through the ionosphere to the ground. For $\psi_0 < \psi_B$, $\psi(\lambda_f)$ becomes very oblique in the negative direction, whereas for $\psi_0 > \psi_B$, $\psi(\lambda_f)$ becomes very oblique in the positive direction. This tendency of the rays to bifurcate at low altitudes based upon their initial ψ has been reported previously [*Chum and Santolik*, 2005; *Santolik et al.*, 2006] and associated with the possible formation of ELF hiss at high latitudes, but inclusion of Landau damping with realistic suprathermal fluxes has not been considered until the present study.

Although the bulk of the chorus power corresponds to rays with $\psi_0 \sim 0°$ [*Bortnik et al.*, 2007], chorus is nevertheless routinely observed with high ψ at the source [*Hayakawa et al.*, 1990] and on low altitude spacecraft (e.g., *Santolik et al.*, [2006]). An example from the DEMETER satellite is shown in Figure 4, observed at an altitude of 709 km. Panels (a)-(d) show the magnetic and electric power spectrograms, and **k**-vector angles ($\psi_{\rm BK}$, azimuth angle relative to $+\mathbf{B}$, $\phi_{\rm BK}$, zenith angle measured anticlockwise relative to $+\mathbf{B}$ with 0° pointing to higher L-shells). The chorus elements contain significant electromagnetic wave power, have clearly propagated to much higher latitudes than typical chorus waves, and have $\psi_{\rm BK} \sim 30°$, similar to the values obtained in Figure 2, column (B). The ray tracing shown in the present paper, as well as previous studies [*Chum and Santolik*, 2005] confirms that these waves are penetrating chorus.

4. Implications for particle scattering

Figure 3 row (d) shows the resonant energies of electrons near the edge of the loss-cone for each ray as a function of latitude [e.g., *Bortnik et al.*, 2006b, Eq. (2)]. Included are co-streaming cyclotron resonances $m = -5$ to -1 (red), the co-streaming Landau resonance $m = 0$ (black), and counter-streaming resonances $m = 1 - 5$ (blue). The dominant $m = 1$ resonance is shown as the thick blue line in each of the plots.

To indicate regions of field-aligned propagation (and hence most efficient wave-particle interaction), we chose an arbitrary limit of $|\psi| = 30°$, and highlighted this region for each ray in rows (c) and (d). As shown, penetrating chorus (B) readily resonates with MeV electrons at $\lambda \sim 30°$ with $\psi \leq 30°$, and may thus contribute to the formation of relativistic electron microbursts [*Lorentzen et al.*, 2001] which have been shown to be an effective radiation-belt loss mechanism [*Thorne et al.*, 2005]. We note that if the wave frequency is decreased (not shown), a greater range of ψ_0 will be able to access high latitudes and scatter MeV electrons into the loss-cone, contributing to microburst formation, but chorus wave power simultaneously decreases and essentially vanishes below $f \sim 0.1 f_{ce}$.

5. Conclusions

Using ray tracing and suprathermal electron distributions from the CRRES satellite, the final propagation latitudes λ_f of typical chorus rays have been calculated as a function of L, MLT, AE, and ψ_0. While the bulk of chorus wave power was previously shown to be consistent with rays injected at $\psi_0 = 0°$ [*Bortnik et al.*, 2007], the present study shows that rays initiated within a certain range of wave normals $\psi_P \sim -0.8\psi_G$ to $-0.6\psi_G$ are able to propagate to very high latitudes and low altitudes ('penetrating chorus'). Penetrating chorus avoids the initial large damping associated with large oblique ψ by quickly rotating towards $\psi \sim 0°$, and also avoids the large damping at mid-latitudes associated with ψ rotating to oblique values. In addition, the relative wave power of penetrating chorus may increase above its initial value due to magnetic field line convergence. An example of chorus waves observed on the DEMETER satellite at an altitude of 709 km was presented, consistent with penetrating chorus.

By considering 4 representative ray paths with $f = 0.3 f_{ce}$, it was shown that penetrating chorus can resonate efficiently with electrons in the > 1 MeV range, and may thus contribute to the previously reported relativistic electron microbursts.

Finally, since penetrating chorus is able to propagate to low altitudes with $\psi \sim 0°$, the chorus observed on the ground does not necessarily need to be guided in field-aligned ducts, but can propagate entirely in an unducted mode. The bifurcation of wave normal angles (and thus ray directions) at low altitudes may further lead to connections with other waves types (e.g., ELF hiss) as suggested by *Parrot et al.*, 2004, *Chum and Santolik* [2005], and *Santolik et al.* [2006].

Acknowledgments. JB and RMT acknowledge support from NSF grants ATM-0402615 and ATM-0621724 (GEM postdoc award), and NASA grants NNG04GM44G and NNG04-G01G through subcontract 17496790-30026-A with Stanford University. NPM would like to acknowledge support from the Natural Environment Research Council, U.K. We also thank NSSDC Omniweb for providing the geomagnetic index data used in the paper. OS acknowledges support from the ESA PECS contract 98025 and GACR grant 205/06/1267.

References

Angerami, J.J., and J.O. Thomas (1964), Studies of Planetary Atmospheres. 1. Distribution of Electrons + Ions in Earths Exosphere, *J. Geophys. Res.*, 69 (21), 4537.

Bortnik J., U. S. Inan, and T. F. Bell (2006a), Landau damping and resultant unidirectional propagation of chorus waves, *Geophys. Res. Lett.*, Vol. 33, Iss. 3, doi:10.1029/2005GL024553.

Bortnik J., U. S. Inan, T. F. Bell (2006b), Temporal signatures of radiation belt electron precipitation induced by lightning generated MR whistler waves. Part I: Methodology, *J. Geophys. Res.*, Vol. 111, A02204, doi:10.1029/2005JA011182.

Bortnik, J., R. M. Thorne, and N. P. Meredith (2007), Modeling the propagation and characteristics of chorus using CRRES suprathermal fluxes, *J. Geophys. Res.*, [sub judis].

Brinca, A.L. (1972), On the Stability of Obliquely Propagating Whistlers, *J. Geophys. Res.*, Vol. 77, No. 19, p. 3495.

Burtis, W.J., and Helliwell, R.A. (1976), Magnetospheric chorus: Occurrence patterns and normalized frequency, *Planet. Space Sci.*, Vol. 24, No. 11, p. 1007-1007.

Carpenter, D.L., and R.R. Anderson (1992), An ISEE/Whistler Model of Equatorial Electron-Density in the Magnetosphere, *J. Geophys. Res.*, 97 (A2), 1097-1108.

Chum, J. and O. Santolik (2005), Propagation of whistler-mode chorus to low altitudes: divergent ray trajectories and ground accessibility, *Ann. Geophys.*, Vol. 23, Iss. 12, pp. 3727-3738.

Hayakawa, M., K. Hattori, S. Shimakura, M. Parrot, and F. Lefeuvre (1990), Direction finding of chorus emissions in the outer magnetosphere and their generation and propagation, *Planet. Space Sci.*, Vol. 38, pp. 135-143, doi:10.1016/0032-0633(90)90012-F.

Horne, R. B., and R. M. Thorne (2003), Relativistic electron acceleration and precipitation during resonant interactions with whistler mode chorus *Geophys. Res. Lett.*, 30, 1527.

Horne, R. B., R. M. Thorne, S. A. Glauert, J. M. Albert, N. P. Meredith, and R. R. Anderson (2005), Timescale for radiation belt electron acceleration by whistler mode chorus waves, *J. Geophys. Res.*, Vol. 110, A03225, doi:10.1029/2004JA010811.

Inan, U.S., and T.F. Bell (1977), The Plasmapause as a VLF Wave Guide, *J. Geophys. Res.*, Vol. 82, No. 19, 2819-2827.

Lorentzen, K. R., J. B. Blake, U. S. Inan, and J. Bortnik (2001), Observations of relativistic electron microburts in association with VLF chorus, *J. Geophys. Res.*, Vol. 106, No. A4, pp. 6,107-6,027.

Meredith, N. P., R. B. Horne, and R. R. Anderson (2001), Substorm dependence of chorus amplitudes: Implications for the acceleration of electrons to relativistic energies, *J. Geophys. Res.*, Vol. 106, No. A7, pp. 13,165-13,178.

Meredith N. P., R. B. Horne, R. H. A. Iles, R. M. Thorne, D. Heynderickx, and R. R. Anderson (2002), Outer zone relativistic electron acceleration associated with substorm-enhanced whistler mode chorus, *J. Geophys. Res.*, 107 (A7), doi:10.1029/2001JA900146.

Meredith, N. P., R. B. Horne, R. M. Thorne, D. Summers, and R. R. Anderson (2004), Substorm dependence of plasmaspheric hiss, *J. Geophys. Res.*, Vol. 109, A06209, doi:1029/2004JA010387.

Parrot, M., O. Santolik, D. A. Gurnett, J. S. Pickett, and N. Cornilleau-Wehrlin (2004), Characteristics of magnetospherically reflected chorus waves observed by Cluster, *Ann. Geophys.*, 22, 2597-2606.

Santolik, O., D.A. Gurnett, and J.S. Pickett (2004), Multipoint investigation of the source region of storm-time chorus, *Ann. Geophys.*, 22, pp. 2555-2563.

Santolik, O., J. Chum, M. Parrot, D. A. Gurnett, J. S. Pickett, and N. Cornilleau-Wehrlin (2006), Propagation of whistler mode chorus to low altitudes: Spacecraft observations of structured ELF hiss, *J. Geophys. Res.*, Vol. 111, Iss. A10, doi:10.1029/2005JA011462.

Thorne R. M., and C. F. Kennel (1967), Quasi-trapped VLF propagation in the outer magnetosphere, *J. Geophys. Res.*, 72, 857-870.

Thorne, R. M., T. P. O'Brien, Y. Y. Shprits, D. Summers, and R. B. Horne (2005), Timescale for MeV electron microburst loss during geomagnetic storms, *J. Geophys. Res.*, Vol. 110, A09202, doi: 10.1029/2004JA010882.

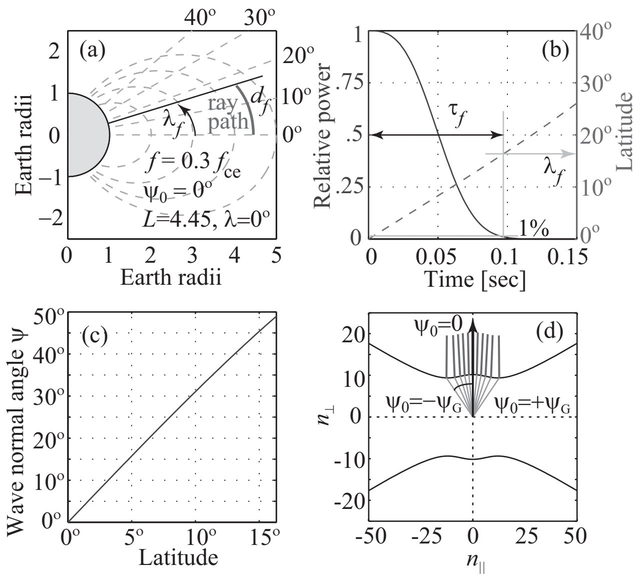

Figure 1. Illustration of ray propagation at $L = 4.45$, MLT = 5.5, $\psi = 0°$, $f = 0.3 f_{\rm ce}$ and AE > 300 nT. (a) ray path; (b) Relative wave power (solid line) and ray latitude (dashed line) vs. group time, showing the 1% power level which defines ray termination, giving $\tau_f = 0.0971$ sec, $\lambda_f = 16.34°$, and $d_f = 1.28 R_E$; (c) $\psi(\lambda)$; and (d) refractive index surface $n(\psi_0)$ showing ψ_0 from $-\psi_G$ to $+\psi_G$, in $0.2\psi_G$ intervals. The wave normal and group vector in panels (a)-(c) is shown as the black line at $\psi = 0°$. $n_{||}$ and $n_\perp$ are the components of the refractive index parallel and perpendicular to the magnetic field, respectively.

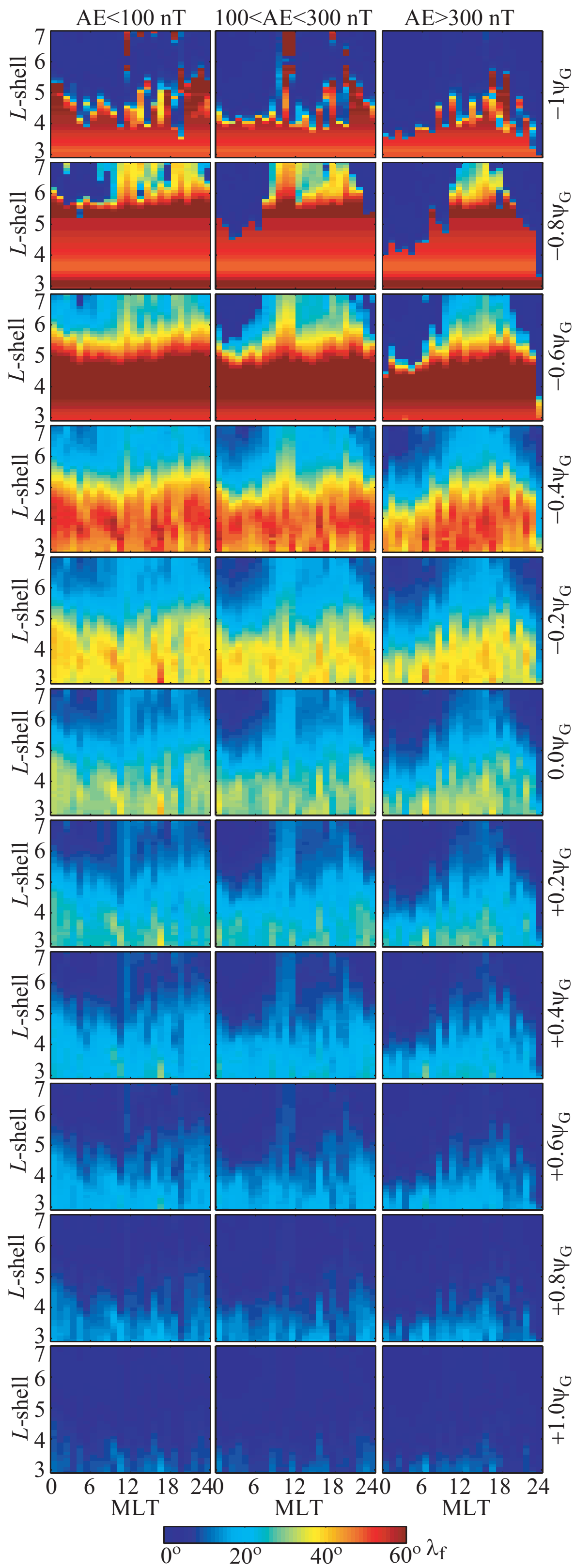

Figure 2. Final propagation latitude λ_f(MLT, L), parameterized by geomagnetic activity and ψ_0.

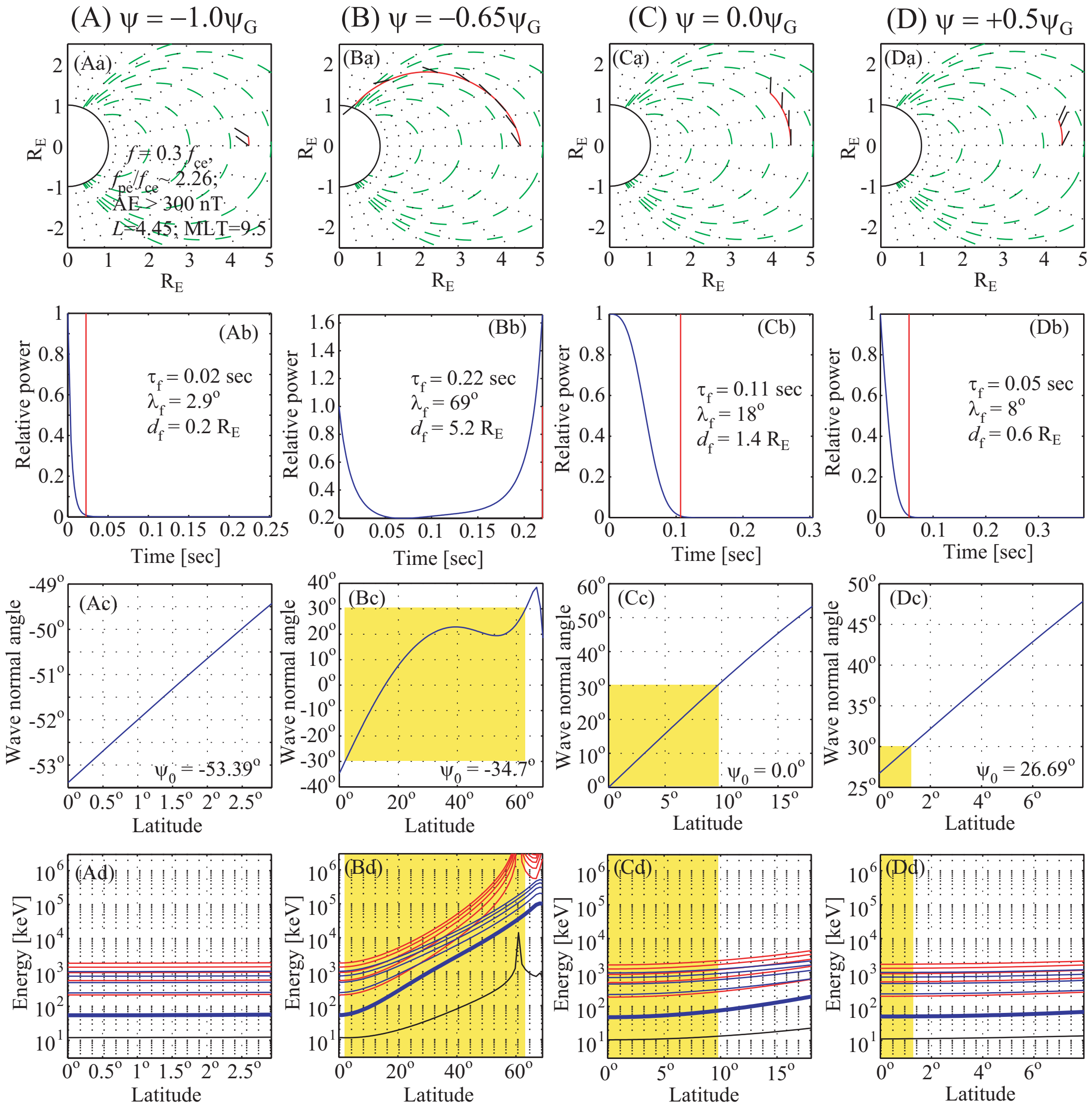

Figure 3. Individual ray characteristics. Columns (A)–(D) correspond to rays injected with $\psi_0 = -1.0\psi_G$, $-0.65\psi_G$, $0.0\psi_G$, and $+0.5\psi_G$ respectively. Rows (a)–(d) correspond respectively to ray path, relative power of the ray vs. group time, $\psi(\lambda)$, and energies of resonant electrons, showing $m < 0$ (red), $m = 0$ (black), and $m > 0$ (blue) resonance harmonics, with the dominant $m = 1$ resonance indicated with a thick blue line.

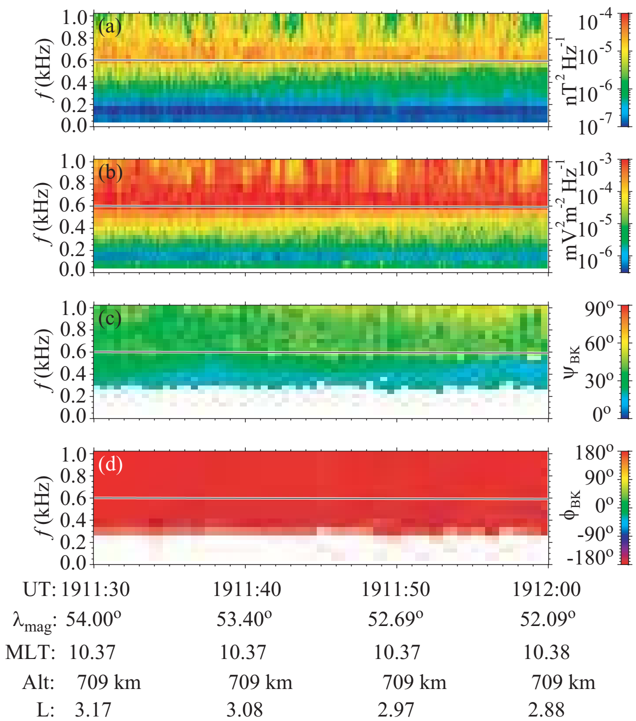

Figure 4. Dynamic spectrogram of chorus elements observed on the DEMETER satellite. (a) wave magnetic field, (b) wave electric field, (c) zenith angle relative to +**B**, and (d) azimuth angle measured anticlockwise about +**B**, with $\phi_{\mathrm{BK}} = 0°$ pointing to higher L-shells. The black line represents the value of the local proton gyrofrequency for reference.